Electronic Supplementary Information for

In-Situ Imaging Lithium Superoxide Dynamics in an All-Solid-State Li-O_2 Nanobattery

Yongfu Tang, [†, ‡, ∇] Tingting Yang, [†, ∇] Jingzhao Chen, [†] Hui Li, [†] Hongjun Ye, [†] Congcong Du, [†]

Yushu Tang, [§] Meirong Xia, [‡, *] Tongde Shen, [†] Liqiang Zhang, [†, *] and Jianyu Huang [†, ⁄⁄, *]

[†]Clean Nano Energy Center, State Key Laboratory of Metastable Materials Science and Technology, Yanshan University, Qinhuangdao 066004, P. R. China.

[‡]Hebei Key Laboratory of Applied Chemistry, School of Environmental and Chemical Engineering, Yanshan University, Qinhuangdao 066004, P.R. China.

[⁄⁄]Key Laboratory of Low Dimensional Materials and Application Technology of Ministry of Education, School of Materials Science and Engineering, Xiangtan University, Xiangtan, Hunan 411105, P. R. China

[§]State Key Laboratory of Heavy Oil Processing, Beijing Key Laboratory of Failure, Corrosion, and Protection of Oil/Gas Facilities, China University of Petroleum Beijing, Beijing 102249, P.R. China.

[∇] Equal Contributors

[*]Correspondence: xmr0125@126.com; liqiangzhang85@163.com; jyhuang8@hotmail.com

Description of Supplementary Movies

Movie S1

Morphology evolution for the formation and shrinkage of spheres during the discharge-charge cycles of the Li-O_2 battery with an Au nanoparticles coated carbon nanotube (Au/CNT) cathode under an annular dark field scanning TEM (ADF-STEM) mode (corresponding to Figure 1, Figures S4-S6). A LiO_2 sphere nucleated and grew along the in-situ formed Li-Au alloy nanoparticle during discharge and shrank immediately during charge. The formation and shrinkage of the spheres were observed several times at different locations on the Au/CNT. The movie was recorded at 5 frames/second, and is played at 1310 × speed.

Movie S2

Morphology evolution for the formation and shrinkage of spheres during the discharge-charge cycles of the Li-O_2 battery with an Au/CNT cathode under an e-beam blank mode (corresponding to Figure S7). Nucleation and growth of LiO_2 spheres along the in-situ formed aggregated Li-Au alloy nanoparticle under a negative potential, and its shrinkage under a positive potential were also observed in an e-beam blank transmission electron microscope (TEM) mode. The movie was recorded at 5 frames/second, and is played at 330 × speed.

Movie S3

Morphology evolution for the formation and shrinkage of spheres during the discharge-charge cycles of the Li-O_2 battery with an Au/CNT cathode under an ADF-STEM mode (corresponding to Figure 2). LiO_2 spheres nucleated and grew along the in-situ formed aggregated Li-Au alloy nanoparticle under a negative potential and shrank immediately under a positive potential. The movie was recorded at 5 frames/second, and is played at 122 × speed.

Movie S4

Morphology evolution for the discharge-charge cycles of the Li-O_2 battery with a bare CNT cathode under ADF-STEM mode (corresponding to Figure S8). Only solid lithium sphere was formed at the triple-phase interface of the CNT cathode during discharge, which is different from that observed in the Au/CNT cathode. The movie was recorded at 5 frames/second, and is played at 224 × speed.

Movie S5

Morphology evolution for the discharge-charge cycles of the Li-O_2 battery with a bare CNT cathode under an e-beam blank TEM mode (corresponding to Figure S9). Only conformal coating on the CNT surface and expansion of CNT were observed on the CNT cathode, which is different from the discharge products in the Au/CNT cathode. The movie was recorded at 5 frames/second, and is played at 241 × speed.

Supplementary Figures

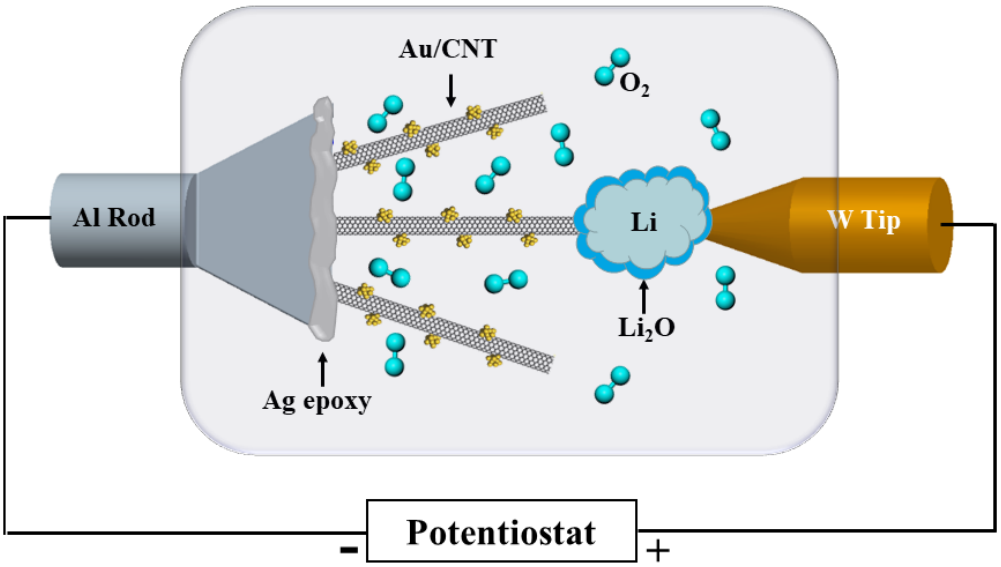

Figure S1. Schematic of the experimental setup for a Li-O_2 nanobattery. The Li-O_2 battery consists of an Au/CNT based O_2 cathode, a Li_2O solid-state electrolyte and a Li anode.

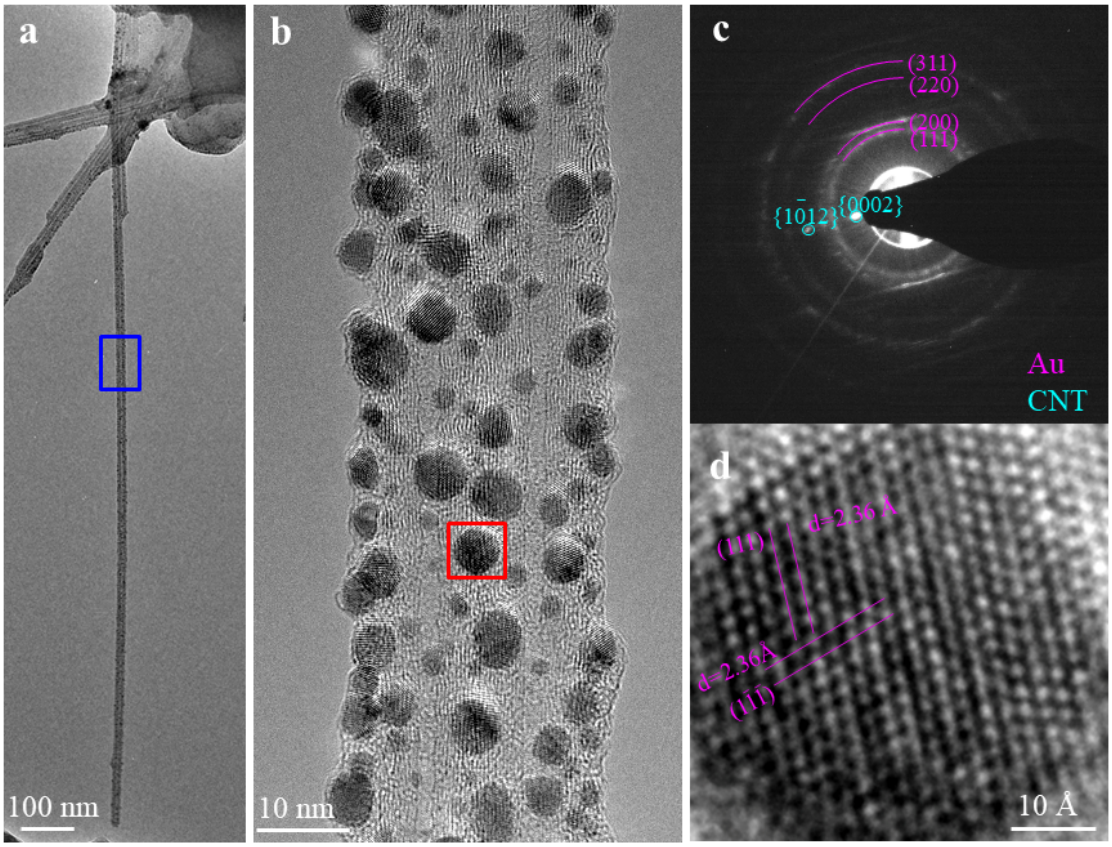

Figure S2. Characterization of the Au/CNT cathode. (a) TEM and (b) high resolution TEM images of the Au/CNT. Au nanoparticles with size of 2 ~ 5 nm were uniformly dispersed on the CNT. (c) EDP of the Au/CNT. The diffraction spots are indexed as CNT (JCPDS card No. 89-8487) and the diffraction rings are indexed as face centered cubic Au (JCPDS card No. 89-3697). (d) High resolution TEM image of the Au nanoparticle.

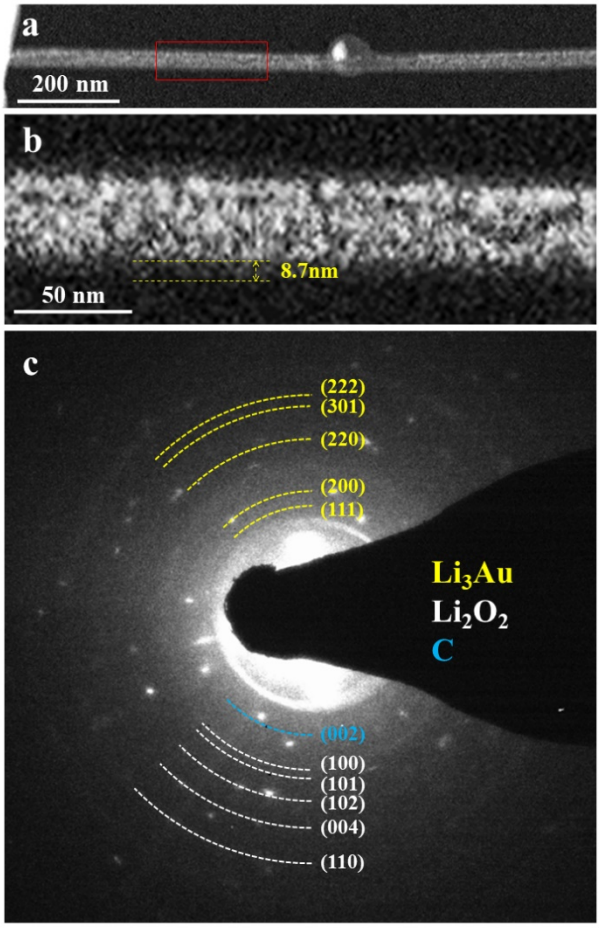

Figure S3. (a) ADF-STEM image of the Au/CNT cathode of the Li-O_2 battery during the discharge process at 2120 s (Figure 1b in manuscript) and (b) the magnified image of the red box region in (a). (c) EDP of the discharge products coated Au/CNT cathode. A conformal coating layer about 8.7 nm was firstly formed on the Au/CNT via lithiation or/and four-electron transferred oxygen reduction reaction. The diffraction rings in the EDP pattern of the product should be ascribed to the (111), (200), (220), (301) and (222) planes of Li_3Au, and the (100), (101), (102), (004) and (110) planes of Li_2O_2, respectively.

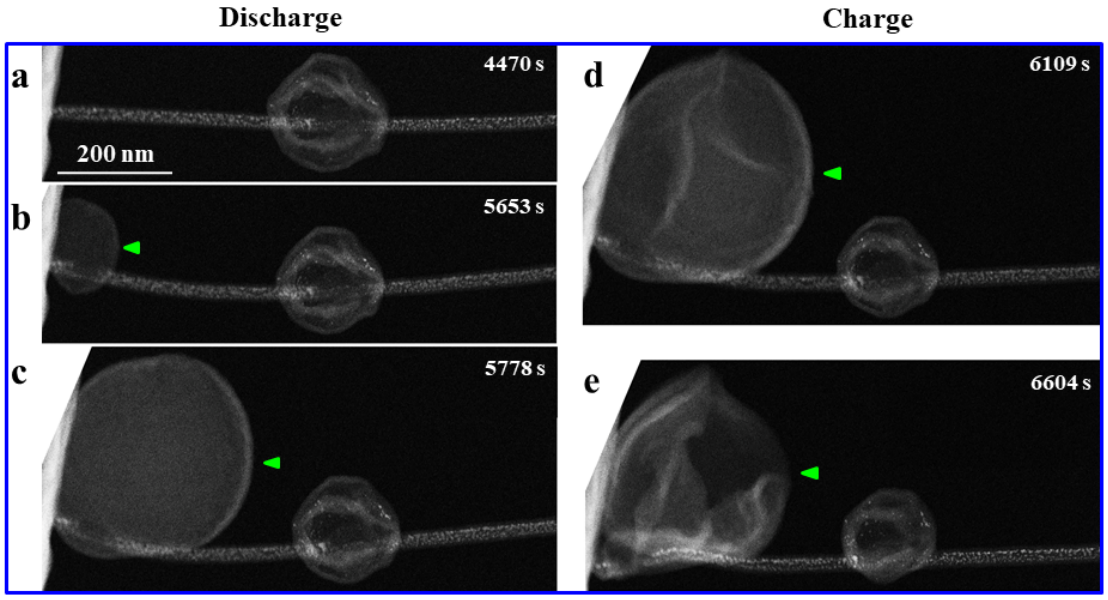

Figure S4. Morphology evolution of the growth and shrinkage of the 2nd LiO_2 sphere during the 2nd discharge-charge cycle of the same Li-O_2 battery as shown in Figure 1 and Movie S1. The sphere nucleated and grew during discharge (a-c), and it immediately shrank during charge (d-e). The sphere pointed out by the green arrowheads was formed and then shrank at this cycle.

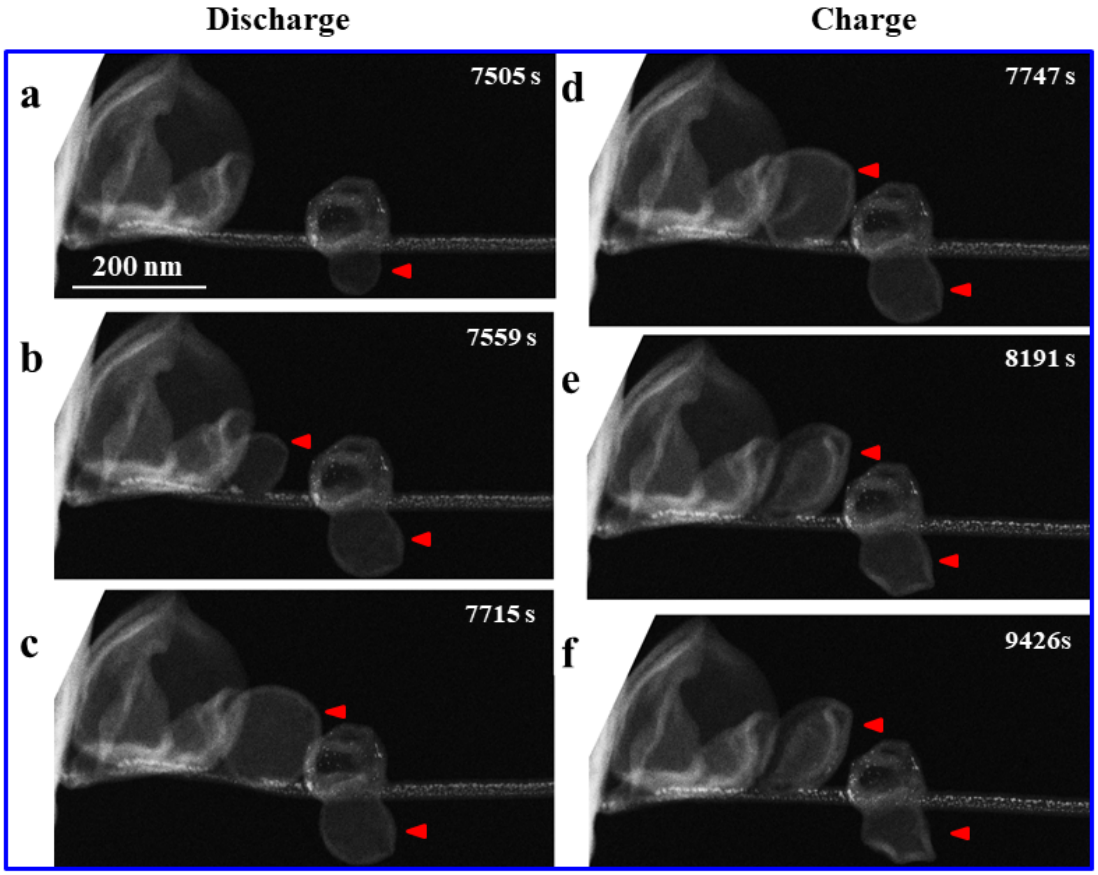

Figure S5. Morphology evolution of the growth and shrinkage of the LiO_2 spheres during the 3rd discharge-charge cycle of the same Li-O_2 battery as shown in Figure 1 and Movie S1. The spheres nucleated and grew during discharge (a-c), and they immediately shrank during charge (d-f). The spheres pointed out by the red arrowheads were formed and shrank at this cycle.

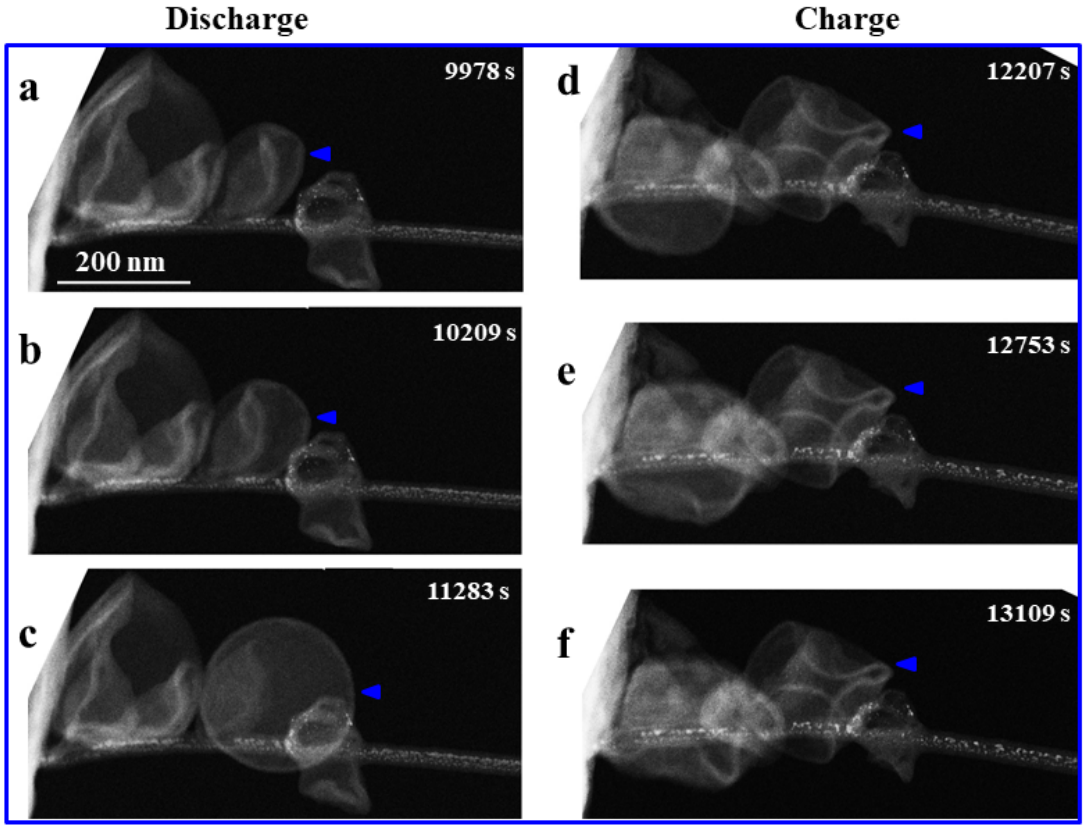

Figure S6. Morphology evolution of the formation and shrinkage of the LiO_2 sphere discharge product on the Au/CNT cathode during the 4th discharge-charge cycle of the same Li-O_2 battery as shown in Figure 1 and Movie S1. The sphere discharge product nucleated and grew under negative potential (a-c), and it immediately shrank under positive potential (d-f). The sphere pointed out by the blue arrowheads was formed and shrank at this cycle.

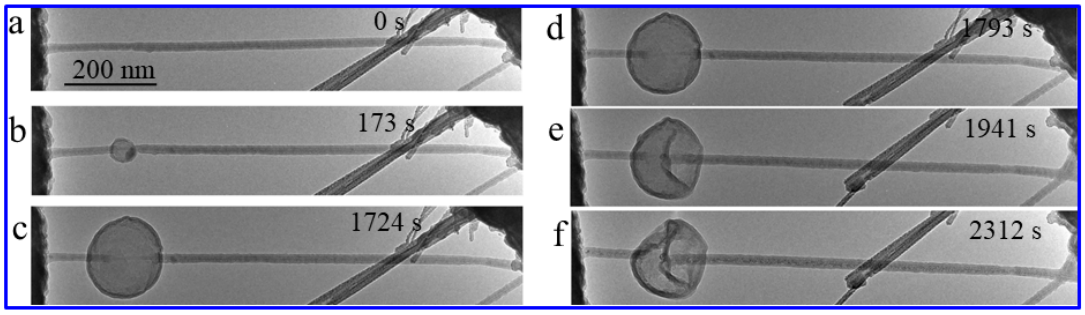

Figure S7. Morphology evolution of (a-c) the formation and (d-f) shrinkage of the LiO_2 sphere discharge product on the Au/CNT cathode under e-beam blank condition corresponding to Movie S2, in which the samples were not showered by the e-beam most of the time except taken images intermittently to avoid the e-beam effect (e-beam blank time is 30 s and the imaging time is 0.5 s).

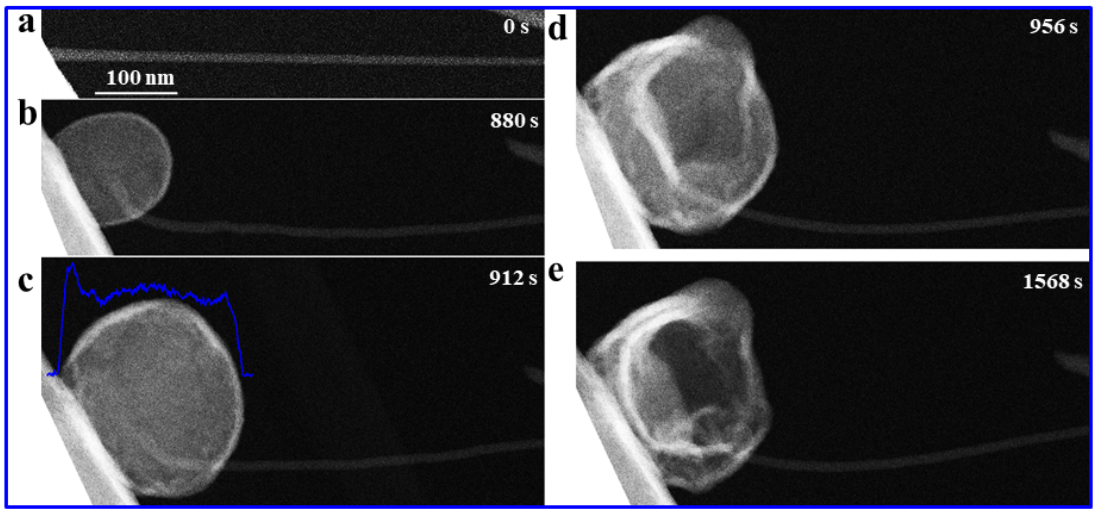

Figure S8. Morphology evolution of CNT cathode without Au nanoparticles during discharge-charge process, corresponding to the Movie S4. A sphere-like discharge product was formed at the site of the three-phase interface under negative potential (a-c), and it shrank under positive potential (d-e). The bump-like intensity profile (blue line) in (c) indicates the solid rather than hollow structure.

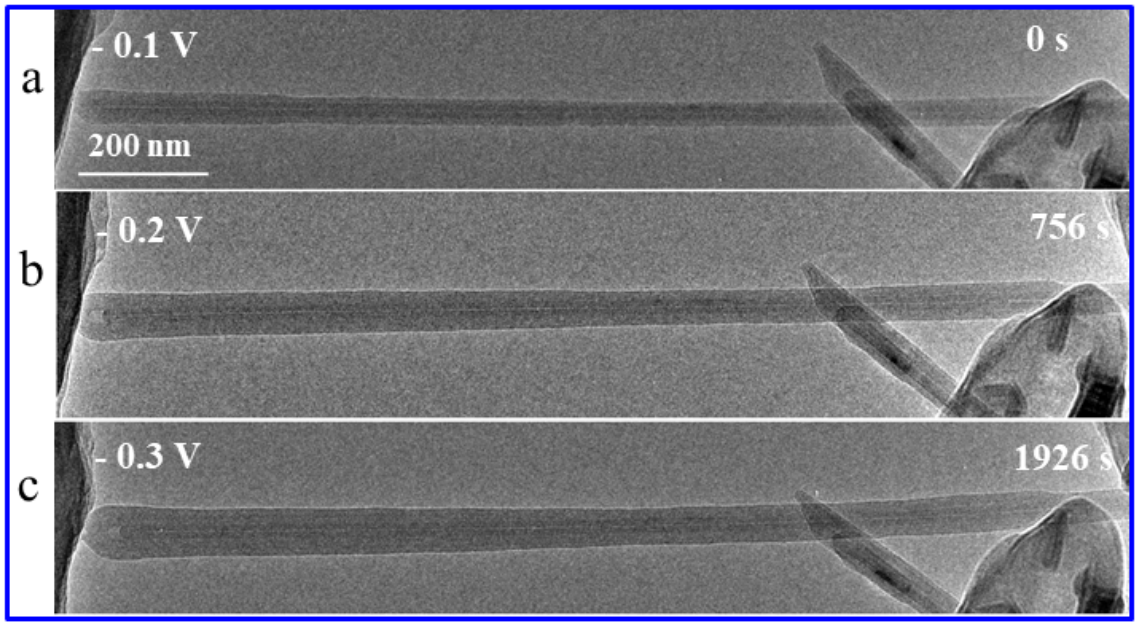

Figure S9. Morphology evolution of the CNT cathode without Au nanoparticles during the discharge-charge, corresponding to the Movie S5. Only a conformal coating layer of Li_2O was formed at the surface of the CNT.

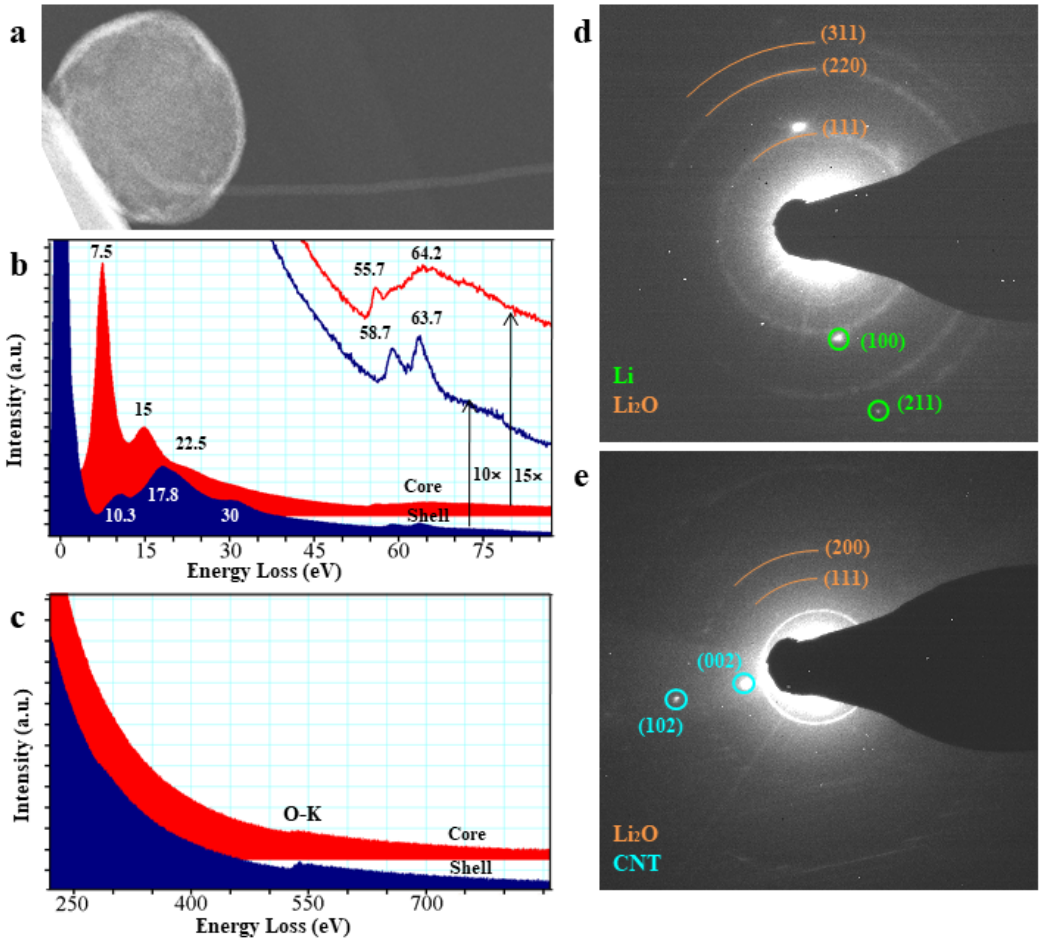

Figure S10. Characterization of the sphere-like discharge product formed on the bare CNT cathode without the Au nanoparticles during discharge. (a) An ADF-STEM image of the sphere, showing a thick shell on the surface. (b) The low-loss Electron Energy Loss Spectroscopy (EELS) spectrum from the core of the ball (red) shows three multiple plasmon peaks at 7.5, 15, and 22.5 eV which agree excellently with that of Li, while that from the shell shows three plasmon peaks at 10.3, 17.8, and 30 eV (blue), which are characteristic peaks of Li_2O. The core-loss EELS from the interior of the ball shows two peaks at 55.7 and 64.2 eV (red), which differs with the peaks at 58.7, and 63.7 eV from Li_2O on the shell (blue). (c) Core-loss spectra of oxygen from the ball interior (red) and the shell (blue), and the former contains a minor oxygen peak originated from Li_2O on the top and bottom surface of the ball. EDPs from the sphere (d) and the CNT (e), which are indexed as Li/Li_2O and Li_2O/CNT, respectively.

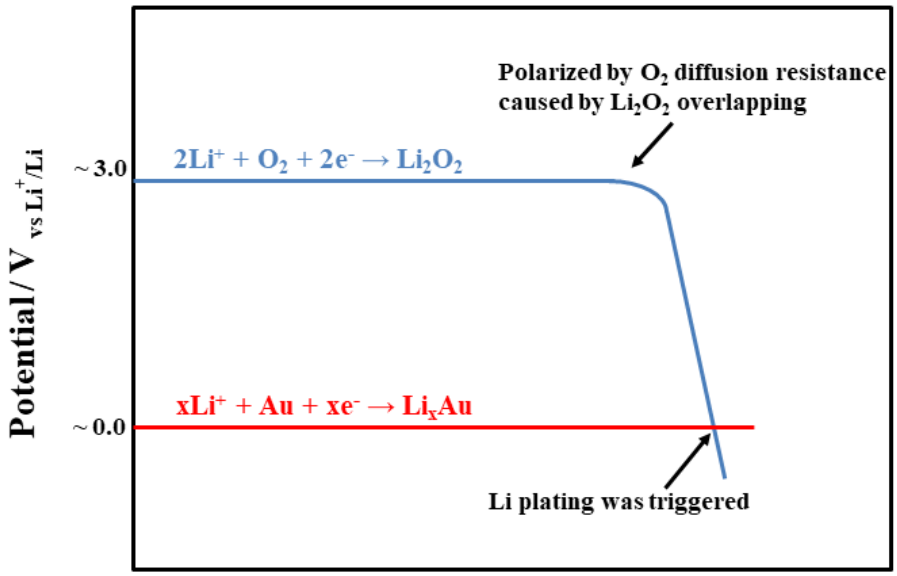

Figure S11. Scheme for the trigger of the electrochemical alloying of Li with Au nanoparticles caused by the severe polarization of the ORR due to the surface Li_2O coating, which prevents the diffusion of O_2.

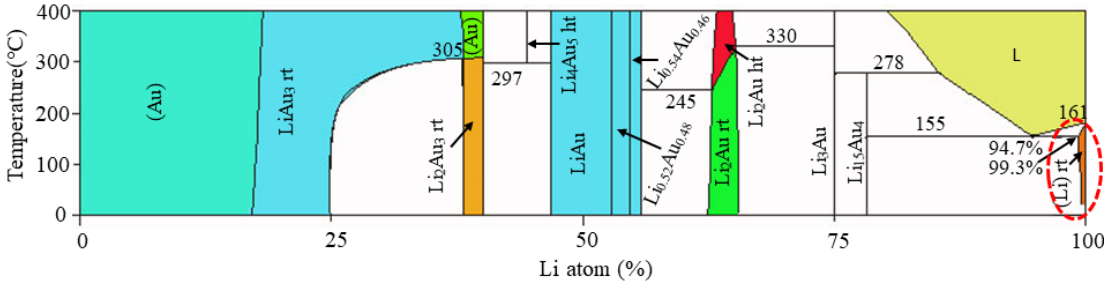

Figure S12. Phase diagram of Li-Au system. Various Li-Au intermetallic compounds and solid solution alloys can be formed with different Li content. The melting point of Li-rich Li-Au alloys is even lower than 200 °C.

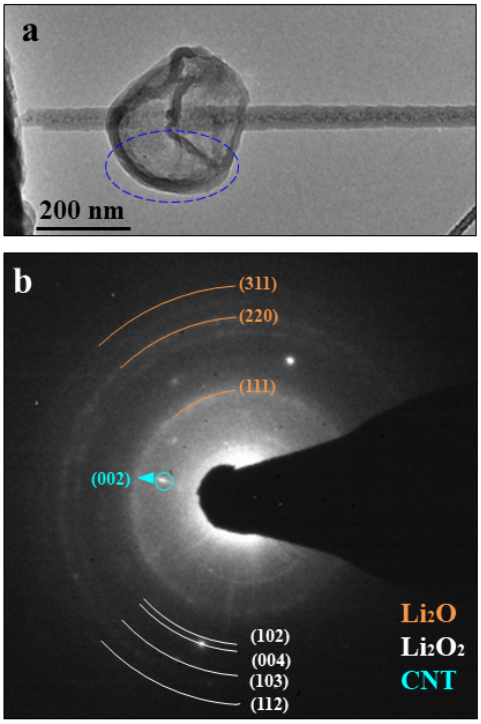

Figure S13 (a) TEM image of the charge products on the Au/CNT cathode and (b) EDP of the shrank sphere.

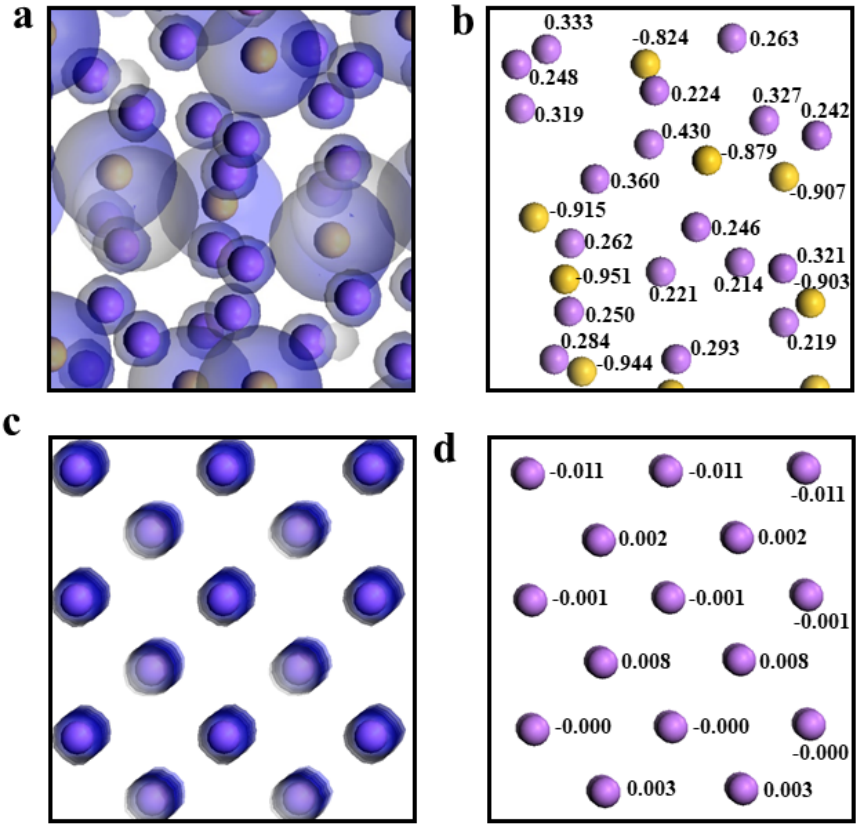

Figure S14. (a) Electron density distribution and (b) net charge of the Li and Au atoms in the pristine $Li_{15}Au_4$; (c) Electron density and (d) net charge of the Li atoms in the pristine Li crystals from the top view of (001) planes. Comparing with that in pure Li, the net charge around Li atoms changes from negative (d) to positive (b) after alloying with Au via transferring its partial active electron into the high-electronegativity Au (χ=2.54), indicating charge transfer from Li to Au. Pink and yellow balls represent for the Li and Au atoms, respectively.

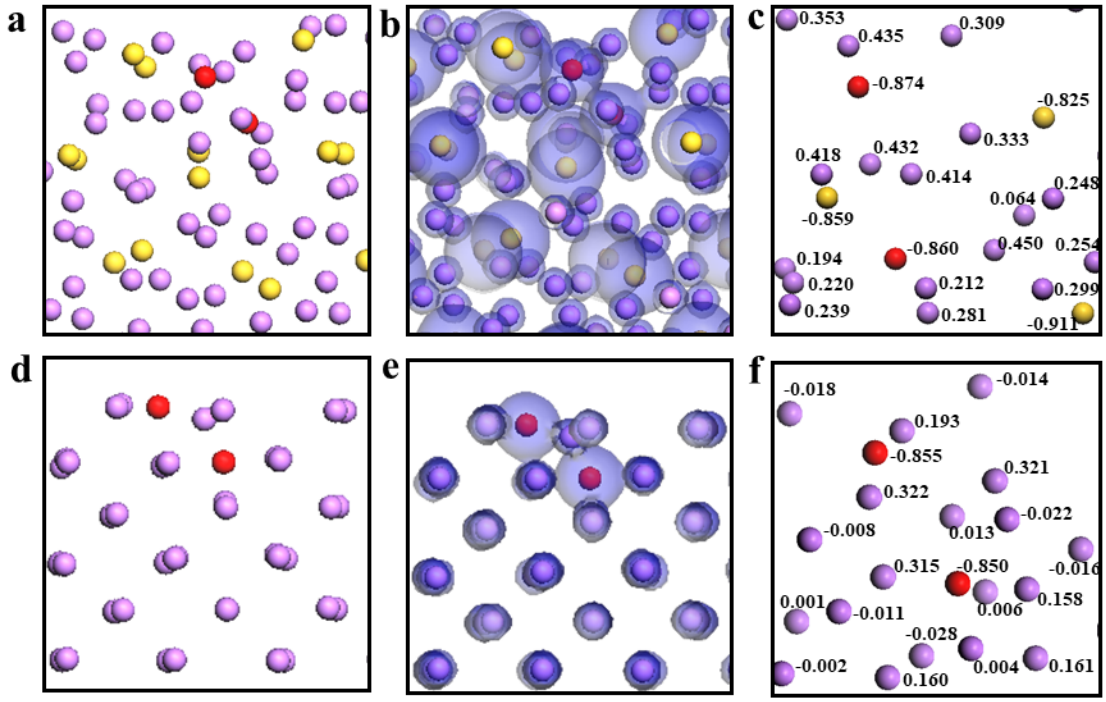

Figure S15. Structure, electron density and net charge of the $Li_{15}Au_4$ (001) and Li (001) with the first dissociated O_2 shown in Figure 5b and g, respectively. (a, d) Sideview of the structure, (b, e) total electron density, and (c, f) net charge of the $Li_{15}Au_4$ (a-c) and the pure Li (d, f), respectively, with the first dissociated O_2. As shown in Figure S14a, b, d, e, the first adsorbed O_2 were dissociated and diffused into the crystal for both $Li_{15}Au_4$ and Li. Net charge of Li atoms around O atoms also change from negative to positive for both $Li_{15}Au_4$ alloy (Figures S14b-c) and pure Li (Figures 14e-f). The electron excess of both Au and O atoms in $Li_{15}Au_4$ (Figure S14c) after the dissolution of the first O_2 (as comparing to the pristine $Li_{15}Au_4$ shown in Figure S13b) indicates the synergistic effect of alloying with Au and the formation of Li-O species in the electron tuning of Li.

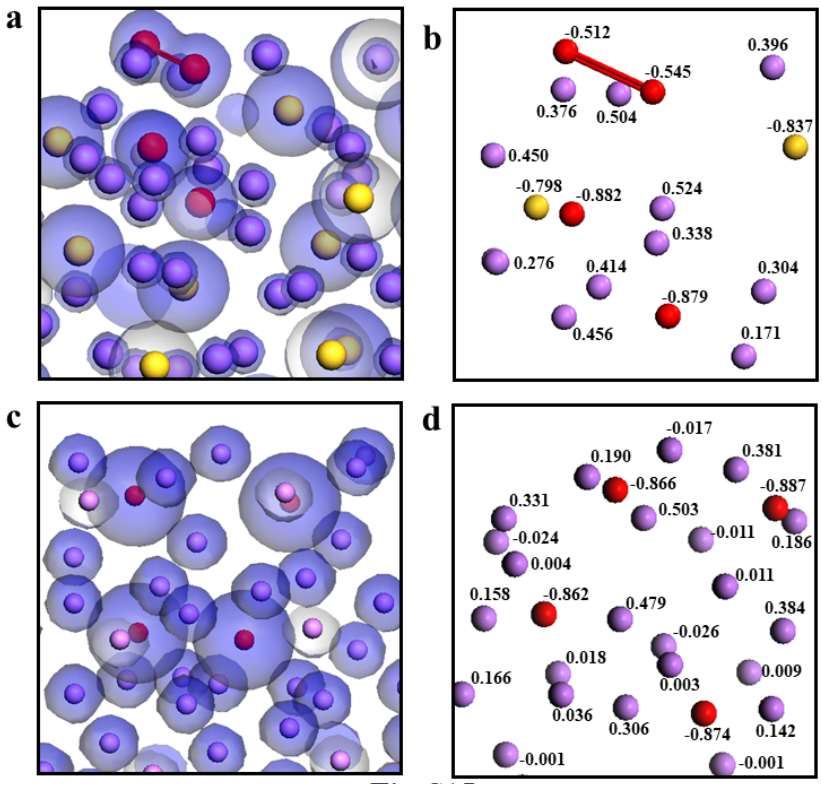

Figure S16. Electron density and net charge of the $Li_{15}Au_4$ and Li with the 2nd adsorbed O_2 on the sites near the Li-O→Au (Site II) and Li-O species in Fig. 5c and 5h, respectively. (a, c) Electron density, and (b, d) net charge for $Li_{15}Au_4$ (a, b) and pure Li (c, d), respectively, after the adsorption of the 2nd O_2. When the 2nd O_2 adsorbed near the top site of Li-O→Au species (Site II) in $Li_{15}Au_4$, LiO_2-like species without cleavage of O-O bond were formed on the surface. By contrast, the 2nd adsorbed O_2 near the top site of the Li-O species in pure Li was further dissociated and diffused into the crystal, similar to the dissociation of the 1st adsorbed O_2 on the pure Li surface. The much lower electron excess (-0.512 and -0.545) , the much shorter O-O distance (1.544 vs 3.126 Å), and the smaller binding energy (-2.73 eV vs ~ 5.3 eV) of the two O atoms from the 2nd adsorbed O_2 than those from the first dissolved O_2 (-0.882 and -0.879) (Figure S15b) confirm its LiO_2-like structure of the 2nd adsorbed O_2 (Table S1). Moreover, the bond angle of the O-Li-O formed from the second adsorbed O_2 (46.59) is much smaller than that formed from the first O_2 (103.82°). It is noted that O-O distance in LiO_2 crystal is 1.344 Å, close to that in the LiO_2-like species. Pink, yellow and red balls represent for the Li, Au and O atoms, respectively.

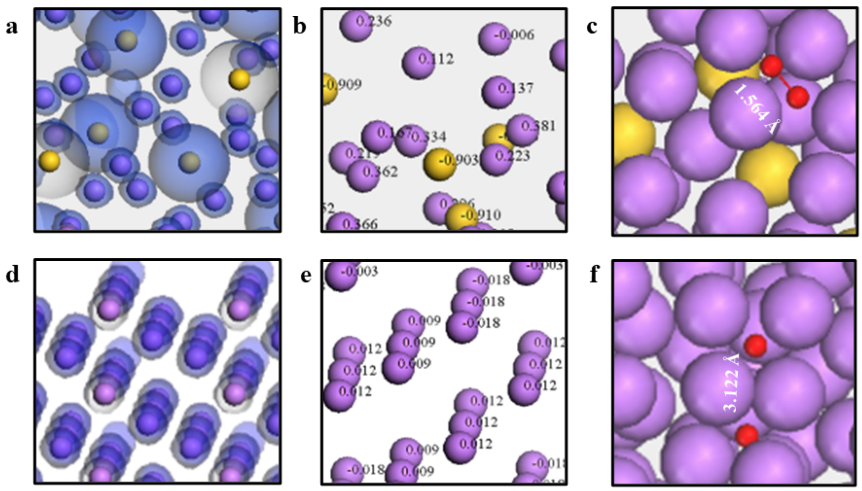

Figure S17 (a, d) Total electron density, and (b, e) net charge for (a, b) $Li_{15}Au_4$ and (d, e) pure Li from the top view of (111) plane, respectively. (c, f) Atomic structure of the (c) $Li_{15}Au_4$ and the (f) pure Li with the adsorbed and relaxed O_2, respectively.

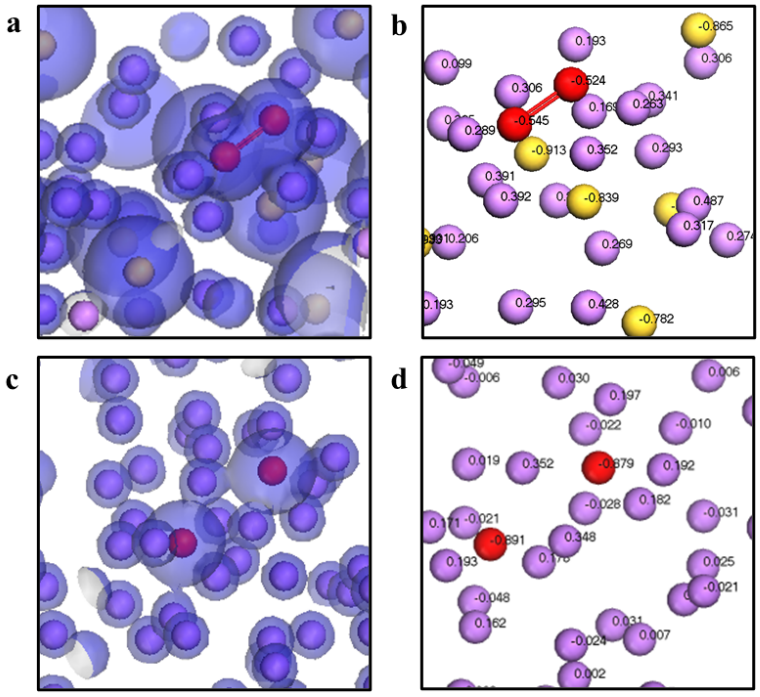

Figure S18 (a, c) Total electron density, and (b, d) net charge of the (a, b) $Li_{15}Au_4$ (111) with the adsorbed O_2 and the (c, d) pure Li (111) with the dissociated O_2, respectively.

Discussion: DFT calculations based on the $Li_{15}Au_4$ (111) and Li (111) confirm that the

formation of LiO_2 is mainly attributed to the de-activation of lithium via electron transfer from Li to Au, which weakens Li's electron donation capability. The formation of LiO_2 has very weak correlation with the exposed planes of the $Li_{15}Au_4$. The electron density and net charge from top view of the $Li_{15}Au_4$ (111) and (001) indicate that the electron transfer from Li to Au atoms is similar on both planes (Figure S17a-b, d-e), suggesting that the charge transfer has little association with the atomic planes. When the O_2 adsorbed on the (111) plane of the $Li_{15}Au_4$, the O-O bond only elongates to 1.564 Å (Figure S17c), which is close to the O-O bond of the adsorbed O_2 on the Li-O→Au covered $Li_{15}Au_4$ (001) surface (1.544 Å) (Figure S16, Table S1). For comparison, the O_2 was dissociated into atomic O with O-O distance of 3.112 Å (Figure S17f) when it was adsorbed on the Li (111). This O-O distance is also close to the result when the O_2 was adsorbed on the Li (001). Furthermore, the net charges of the O atoms in the $Li_{15}Au_4$ (111) (-0.524 and -0.545) are more positive than that in the pure Li (111) (-0.879 and -0.891), suggesting the poor electron donation capacity of Li after the formation of $Li_{15}Au_4$ alloy (Figure S18). All these results indicate that the formation of LiO_2 is mainly attributed to the de-activation of lithium via electron transfer from Li to Au, which weakens Li's electron donation capability, and it has only weak correlation to the planes of the $Li_{15}Au_4$. To keep the brevity of the manuscript, we mainly discuss the electron effect on the formation of LiO_2 with short discussion on the minor effect of planes.

Supplementary Tables

Table S1 Li-O binding energies, Li-O bond distances, O-O distances and bond angles of O-Li-O in the stable structures after the O_2 adsorptions on the Li and $Li_{15}Au_4$ crystals.

Stable structures in Figure 5	Li-O binding energy (eV)	Li-O bond distance (Å)	O-O distance (Å)	O-Li-O bond angle (°)
Adsorption of 1st O_2 on Site I of $Li_{15}Au_4$ (Figure 5b)	-5.17	1.927	3.126	103.82
Adsorption of 2nd O_2 on Site II of $Li_{15}Au_4$ (Figure 5c)	**-2.73**	_	**1.544**	**46.59**
Adsorption of 2nd O_2 on Site II' of $Li_{15}Au_4$ (Figure 5d)	-5.04	1.930	3.178	112.78
Adsorption of 3rd O_2 on Site III of $Li_{15}Au_4$ (Figure 5f)	**-2.06**	_	**1.487**	**42.37**
Adsorption of 1st O_2 on Li (Figure 5g)	-5.45	1.897	2.774	91.30
Adsorption of 2nd O_2 on Li (Figure 5h)	-5.43	1.898	3.186	114.58
Adsorption of 3nd O_2 on Li (Figure 5i)	-5.37	1.902	3.242	120.74

Discussion: As shown in Table S1, the Li-O binding energies, O-O distances and O-Li-O bond angle of the structure formed after the adsorptions of 2nd O_2 on Site II and the 3rd O_2 on site III on $Li_{15}Au_4$ are about half of those from the structures formed on pure Li after adsorptions of O_2, indicating that LiO_2-like species is formed on the Li-O→Au surface, while Li_2O-like species is formed on the pure Li surface and diffused into the Li crystal. The more detailed discussions were given in Figures S14-S16.